Experimental Investigation of H_2-Brine Relative Permeability in Tight Sandstone for Assessing Underground Hydrogen Storage Efficiency

Bettina Jenei[1], *Wael F.* Al-Masri[2*], *Souhail* Youssef[3], *Basil* Alwardy[1], *Birger* Hagemann[1], and *Leonhard* Ganzer[1]

[1] Clausthal University of Technology, Institute of Subsurface Energy Systems, 38678 Clausthal-Zellerfeld, Germany
[2] Geological Survey of Denmark and Greenland (GEUS), Department of Geo-energy and Storage, 1350 Copenhagen K, Denmark
[3]IFP Energies Nouvelles, 1 et 4 avenue de Bois-Préau, 92852 Rueil-Malmaison, France

Abstract. Underground hydrogen storage (UHS) in depleted hydrocarbon reservoirs and other porous formations such as aquifers is increasingly considered a key large-scale energy buffer for supporting intermittent renewable energy systems. Reliable prediction of hydrogen injectivity, migration, trapping, and recovery efficiency requires robust multiphase flow characterisation, particularly H_2 brine relative permeability. However, hydrogen's low density, high diffusivity, and distinct interfacial properties introduce displacement behaviours that differ fundamentally from those of CO_2 or N_2 based analogues. Experimental datasets for H_2 brine systems, especially in tight sandstones, remain scarce due to operational complexity, hydrogen safety constraints, and measurement uncertainties under low permeability conditions. This study presents primary drainage H_2 brine relative permeability measurements on tight sandstone core plugs spanning a permeability range representative of aquifers originated from depleted gas reservoir intervals considered for UHS. Unsteady state core flooding experiments were conducted in a laboratory approved for hydrogen use equipped with detection, ventilation, and safety control systems, with relative permeability curves derived from measured flow rates and brine production using history matching. The resulting functions exhibit pronounced permeability dependence and systematic differences relative to published CO_2-brine and N_2-brine analogue datasets attributable to hydrogen's distinct fluid properties. These findings demonstrate that directly transferring analogue gas brine relative permeability data to UHS simulations may lead to significant predictive errors in injectivity, pressure evolution, and working gas capacity, underscoring the necessity of fluid and permeability specific parameterisation for reliable UHS performance modelling.

1 Introduction & Literature Review

Hydrogen has been identified as a key energy carrier in the transition toward low-carbon energy systems, offering versatility across power generation, industry, transport, and heating, as well as the potential for long-term seasonal storage to balance intermittent renewable electricity supply [1, 2]. Today, hydrogen is produced primarily from natural gas via steam methane reforming at approximately 9 kg CO_2 per kg H_2 and is consumed mainly in refining and petrochemical applications [3]. Scaling up low-carbon hydrogen production, whether from renewable electricity, fossil fuels with carbon capture, or geological sources, requires a parallel development of large-scale storage infrastructure [1, 3].
Among the available storage options, underground hydrogen storage (UHS) in porous geological formations offers the largest capacity potential, reaching the terawatt-hour scale needed for utility-level seasonal balancing, far exceeding the gigawatt-hour capacity of salt caverns or the megawatt-hour scale of surface tanks [5, 6]. Interest in UHS has grown considerably over the past decade, with the number of published studies increasing exponentially since 2021 [4]. Depleted hydrocarbon reservoirs and deep saline aquifers are considered the most practical candidates, given their well-characterised geological frameworks, existing infrastructure, and proven seal integrity [6]. Among these, depleted gas reservoirs hosted in tight sandstone formations are of particular relevance, especially in central Europe, where a significant share of the legacy gas reservoir inventory is characterised by permeabilities in the low tens of millidarcy range. These reservoirs offer established injection and production infrastructure and well-documented geological seals, making them attractive near-term candidates for UHS deployment. However, the tighter pore structures of these formations introduce additional complexity relative to higher-permeability aquifer systems. Elevated capillary entry pressures restrict primary drainage of brine from smaller pores, capillary end effects complicate the accurate derivation of two-phase flow functions from core-scale experiments, and the lower absolute permeabilities amplify the practical consequences of any uncertainty in the relative permeability functions used for injectivity and capacity simulation.
UHS in porous media involves a complex interplay of coupled mechanisms that must be well understood before any storage project can be safely and economically operated [7]. These include hydrodynamic phenomena

* Corresponding author: bettina.jenei@tu-clausthal.de

such as relative permeability, displacement efficiency, viscous fingering, and residual trapping, as well as hydrogen dissolution in brine, geomechanical effects, geochemical reactions with reservoir minerals, and microbial activity [7, 8]. Hydrogen-metabolising microorganisms can consume injected hydrogen, cause biofouling, and corrode infrastructure, and are known to thrive under a wide range of reservoir conditions [8]. Formation evaluation using both routine and special core analysis is therefore critical to assessing the feasibility of a UHS site [7]. Among the hydrodynamic parameters, relative permeability functions for the hydrogen-brine system are relevant only in reservoirs with a significant mobile water phase, such as those with active water drive or where brine has not been fully displaced from the pore space. In depleted gas reservoirs with residual water saturation and in saline aquifers, both phases remain mobile during hydrogen injection and withdrawal, making accurate characterisation of the hydrogen-brine relative permeability essential. These functions describe the simultaneous flow of hydrogen and brine as a function of fluid saturation and directly control injectivity, working gas capacity, and pressure build-up during injection and withdrawal cycles. The physical properties of hydrogen make it a particularly challenging fluid in this regard. Compared to CO_2 and CH_4, hydrogen has a very low molecular weight (2.016 g/mol), a low density (0.082 kg/m³ at 25°C, 1 atm), and a low viscosity (0.89×10^{-5} Pa·s), which is lower than both CO_2 (1.49×10^{-5} Pa·s) and CH_4 (1.1×10^{-5} Pa·s), while its diffusivity in water is three orders of magnitude higher than that of methane [9]. These properties produce a highly unfavourable mobility ratio during brine displacement and increase the risk of viscous fingering, with implications for displacement efficiency and sealing that have no direct analogue in the CO_2 storage literature [9]. Furthermore, hydrogen's wide flammability range in air (4 to 75 vol%) and low ignition energy impose strict requirements on laboratory infrastructure. The experiments presented in this study were conducted in a dedicated facility approved for hydrogen use at the Institute of Subsurface Energy Systems, Clausthal University of Technology, and the safety measures implemented are described in Section 2.3.

1.1 State of the Art

Despite their importance, experimental measurements of H_2-brine relative permeability remain scarce, with fewer than 10 studies published as of 2025 [7]. The first reported measurement was presented by Yekta et al. [10], using Vosges sandstone (ϕ=19%, k=45mD) under shallow- and deep-reservoir conditions via steady-state and modified semi-dynamic methods. Their results showed a connate water saturation of approximately 40% under the steady-state method, reduced to 13% when interpreted via the semi-dynamic approach and capillary pressure, with no significant effect of pore pressure on the k_r curves [10]. Later, Lysyy et al. [11] and Boon and Hajibeygi [12] reported steady-state primary drainage k_r measurements with saturation profile monitoring on Berea sandstone cores of 100 mD and 200 mD, respectively. These studies found higher connate water saturations of around 60%, lower end-point k_r values, and low crossover saturation points, indicating strong phase interference between hydrogen and brine. The imaging results of Boon and Hajibeygi [12] further revealed heterogeneous saturation distributions driven by gravity segregation and capillary barriers, and showed that meaningful k_r parameters can only be extracted from the core's central region.

A more systematic study was presented by Rezaei et al. [13], who measured primary drainage H_2-brine k_r by unsteady-state flooding on sandstone and carbonate samples across a range of pressures and brine salinities. Their results showed that rock type has the largest influence on k_{rg}, while brine concentration has little effect. H_2 was found to have a higher k_r at near-ambient pressure compared to higher pressures, and H_2 and N_2 were found to produce broadly similar k_{rg} curves under primary drainage conditions [13]. However, pore-scale imaging studies on residual trapping demonstrated that H_2 imbibition recovery differs clearly from that of N_2, with hydrogen withdrawal decreasing with increasing pressure, suggesting that deeper reservoirs are less favourable for efficient H_2 recovery [14]. Boon et al. [15] further showed that during storage periods, hydrogen ganglion sizes increase due to Ostwald ripening, which can reduce residual saturation and k_r hysteresis, a potentially beneficial mechanism for working gas recoverability. A similar conclusion was reached by Goodarzi et al. [16].

Across the existing literature, residual hydrogen saturation under primary drainage conditions has generally been found to be low, suggesting that capillary trapping does not pose a fundamental threat to storage efficiency [7]. Nevertheless, all published primary drainage k_r datasets have been obtained on relatively high-permeability samples under conditions representative of saline aquifer storage, and no measurements have been reported for the tighter sandstone systems relevant to depleted gas reservoir targets in central Europe. Using CO_2-brine or N_2-brine analogues as direct proxies for H_2-brine k_r in UHS simulation without correction for the distinct fluid properties of hydrogen would introduce systematic errors in injectivity and capacity predictions, particularly in tighter reservoir intervals where capillary forces are dominant [7, 13]. This study addresses this gap by presenting H_2-brine primary drainage relative permeability measurements on two tight sandstone core plugs from the North German Basin with brine absolute permeabilities of 0.295mD and 0.685mD. Unsteady-state core flooding experiments were conducted at constant pressure difference in a laboratory approved for hydrogen use, and relative permeability functions were derived using both the analytical JBN method and numerical history matching with the Corey model, which explicitly accounts for hydrogen compressibility and capillary end effects. The results are discussed in the context of available literature data, with implications for UHS injectivity assessment, working gas capacity estimation, and field-scale bio-reactive simulation.

2 Materials and Methods

2.1. Rock Samples

Two cylindrical core plug samples (3 cm diameter, up to 6 cm length) were provided by the Institute of Applied Geosciences, Technische Universität Darmstadt, for the purpose of H_2-brine relative permeability measurements in support of underground hydrogen storage simulations. The samples originate from the Buntsandstein, a Lower to Middle Triassic fluvial to aeolian sandstone sequence well documented across the North German Basin as a potential UHS target, and were selected on the basis of their petrophysical properties as the most suitable to fill the gap in the literature, representative of a permeability range for which no H_2-brine relative permeability data currently exist. The samples were collected from depleted hydrocarbon reservoir as analogue samples representing potentials aquifers in the region. The petrophysical properties of both samples are summarised in Table 1.

Table 1. Petrophysical characterisation of the core samples used in this study.

Sample name	Core 3	Core 4
Porosity [%]	13.74	13.31
K_{brine} [mD]	0.295	0.685
K_{gas} N_2[mD]	0.460	0.746
K_{gas} H_2 [mD]	0.522	0.793

Porosity was determined by helium pycnometry using an AccuPyc device, and gas permeabilities were measured under a net confining pressure of 40 bar, to ensure linear fluid flow.

All plugs were drilled perpendicular to bedding to minimize anisotropy effects and to avoid visible natural fractures or macroscopic heterogeneities that could compromise the assumption of one-dimensional linear flow during the flooding experiments.

2.2 Fluids

The aqueous phase used in all experiments was a synthetic brine composed of 4 wt% NaCl dissolved in distilled water, formulated to approximate the salt concentration of the formation water associated with the target reservoir. The brine was prepared using analytical-grade NaCl and filtered. The density and viscosity of the brine at the experimental temperature of 20°C were 1026 kg/m³ and 1.07 mPa·s respectively.

Hydrogen used in the flooding experiments had a certified purity of 99.999% (grade 5.0) and was sourced from a pressurised gas cylinder. As a compressible gas, hydrogen fluid properties were evaluated at the log mean pressure of the experiment, calculated from the inlet pressure of 7.9 bara and the outlet back-pressure of 3 bara, giving a log mean pressure of approximately 5 bar. At these conditions and a temperature of 20°C, hydrogen has a density of approximately 0.414 kg/m³ and a dynamic viscosity of 0.89×10^{-2} mPa·s (0.0089 mPa·s), giving a mobility ratio relative to brine that is highly unfavourable for displacement and may result strong fingering instead of a stable displacement front. The relevant fluid properties at experimental conditions are summarised in Table 2.

Table 2. Fluid properties of hydrogen and synthetic brine evaluated at log mean pressure conditions (5 bar, 20°C).

Property	H2	N2	Brine
Density [kg/m³]	0.414	5.75	1026
Dynamic viscosity [mPa·s]	0.0089	0.0175	1.07

2.3 Laboratory setup and safety

Conducting core flooding experiments with hydrogen requires special safety measures due to its physicochemical properties. Hydrogen exhibits a pronounced leakage potential resulting from its very small molecular size, high diffusivity, and low viscosity. Consequently, the gas can escape even through the smallest leaks and rapidly disperse into the surrounding environment. At the same time, hydrogen is significantly lighter than air, so released gas tends to rise and may accumulate near the ceiling, particularly in regions with limited air circulation. Hydrogen forms flammable and explosive mixtures with air over a very wide concentration range of approximately 4 to 77%. The minimum ignition energy is only about 0.02 mJ, which is significantly lower than the energy of typical electrostatic discharges, meaning that even very small sparks can serve as ignition sources. The autoignition temperature is approximately 560°C. This combination results in a significant hazard, especially in high-pressure core flooding experiments where large quantities of hydrogen are required. To ensure safe operation of the experimental setup, additional technical and organisational measures were implemented based on a comprehensive risk assessment and the preparation of a binding operating instruction. All components of the core flooding setup that come into contact with hydrogen, including the core holder, differential and absolute pressure sensors, and the control panel with valves, were installed inside a well-ventilated fume hood, ensuring that any escaping hydrogen is immediately captured by the directed airflow and safely removed without entering the laboratory environment. The hydrogen cylinder and all other gas cylinders are stored in a separate gas cylinder cabinet connected to the same ventilation system as the fume hood. To minimise ignition risks, the relevant areas were formally classified as Zone 2 hazardous areas, and all

electrical components used within these zones are rated for operation in potentially explosive atmospheres. The pressure sensors are operated via certified intrinsic safety barriers. The injection pumps are decoupled from the hydrogen flow path using floating piston accumulators, placing the pumps outside the hazardous zone. For early detection of potential hydrogen releases, a dedicated gas detection system was installed with multiple sensors positioned at critical locations: in the upper section of the fume hood, in the upper section of the gas cylinder cabinet, below the laboratory ceiling, and in the area of the gas pressure regulators. The system triggers an alarm at 20% of the lower explosive limit and simultaneously initiates an automatic safety shutdown by interrupting the hydrogen supply via a solenoid valve. Prior to the initial filling of the system with hydrogen, a leak test using nitrogen was carried out to identify any potential leakage points. A sketch of the complete experimental setup is shown in Figure 1.

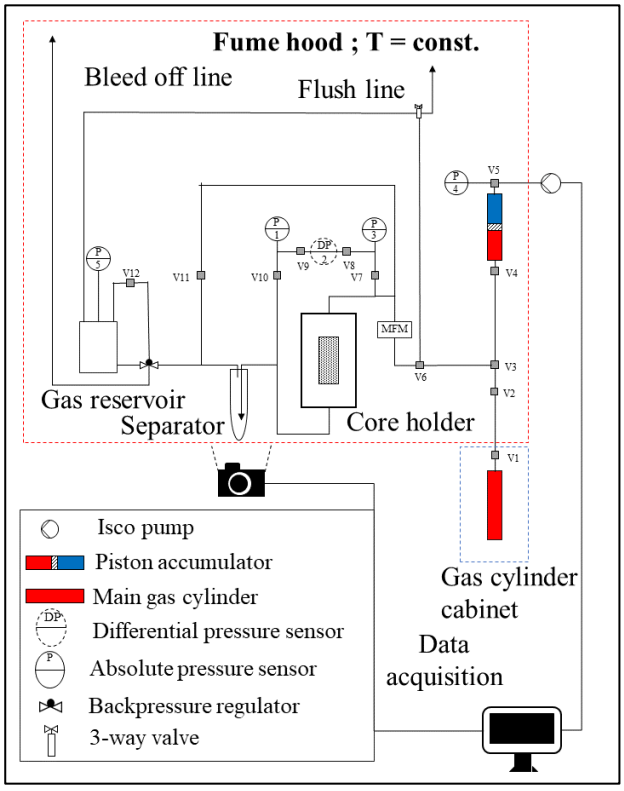

Fig. 1. Schematic diagram of the H2-brine USS experimental setup.

Through this combination of design, technical, and organisational measures, the risks associated with the use of hydrogen in the core flooding experiments presented here are significantly reduced, allowing for the safe and reliable execution of the measurements. The central component of the apparatus is a Hassler-type core holder accommodating samples with a diameter of 3 cm and a length of up to 6 cm. Pressure sensors installed on both sides of the core sample record the differential pressure across the core continuously throughout each experiment. The injection pump is decoupled from the hydrogen flow path using a floating piston accumulator. Additionally, the experimental setup is not restricted to near-ambient conditions, low pressure and temperature were chosen to prioritise safety at this stage, where the risks associated with compressing and heating the hydrogen system were minimised, with the intention of extending measurements to representative reservoir conditions in future work.

2.4 Core-flooding procedure

Prior to each measurement, the core sample was fully saturated with the 4 wt% NaCl brine solution under vacuum to achieve complete pore saturation (S_w=1.0), confirmed gravimetrically, and then placed into the Hassler cell. The core was mounted vertically, with flow directed from top to bottom, so that the injection of hydrogen, the less dense non-wetting phase, proceeds in the direction of gravity. This configuration was chosen to promote a more stable displacement front and to minimise the effect of gravity segregation at the inlet that has been reported in horizontal flooding experiments with hydrogen [12]. A confining (radial) pressure of 40 bar was applied to ensure linear flow conditions and to prevent bypass of fluids along the core sleeve. The absolute brine permeability was determined at this stage by injecting brine at a constant pressure difference and applying Darcy's law to the stabilised flow rate. The unsteady-state primary drainage experiment was initiated by applying a constant pressure difference of 4.9 bar across the core, with the inlet pressure maintained at 7.9 bara and the outlet back-pressure held at 3 bara, giving a log mean pressure of approximately 5 bar. Under these conditions, hydrogen was injected continuously, and the resulting flow rate varied with time as the saturation distribution within the core evolved. The differential pressure across the core was recorded continuously by the inlet, outlet, and differential pressure sensors. The volume of displaced brine produced at the outlet was collected and measured alongside the mass of the injected gas throughout the experiment. All measurements were conducted at a temperature of 20°C. The experiment was terminated once the transient flow period had been reached and no further brine production was observed over a sustained period, consistent with the approach recommended in the literature [21]. Stable conditions were achieved after approximately 320 minutes for Core 3 and 150 minutes for Core 4.

2.5 Relative Permeability Interpretation

2.5.1 Analytical approach (JBN).

The JBN method [19], extended using the graphical technique of Jones and Roszelle [20] and based on Buckley-Leverett theory, was applied as a base case analytical interpretation and as the starting point for the numerical history matching. This approach assumes immiscible two-phase flow and neglects capillary pressure between the phases, but account for gas compressibility. Under the constant pressure difference condition applied in this study, the total flow rate varies

with time as the saturation distribution evolves within the core. The fractional flow function, and the relative permeability ratio are derived directly from the measured gas flow rate at the inlet, the cumulative production data and the pressure difference as follows:

$$u_w(L,t) = (1/A) \cdot dQ_w/dt \quad (1)$$

$$u_{nw}(L,t) = (1/A) \cdot dQ_{nw}/dt \quad (2)$$

$$S_w(L,t) = S_{wc} + (1/AL\varphi) \cdot (t \cdot dQ_w/dt - Q_w(t)) \quad (3)$$

$$k_{rw} / k_{rnw} = (\mu_w/\mu_{nw}) \cdot (u_w/u_{nw}) \quad (4)$$

$$k_{rw} = (\mu_w \cdot L \cdot u_w)/K \cdot (\Delta P - t \cdot d\Delta P/dt)^{-1} \quad (5)$$

$$k_{rnw} = (\mu_{nw} \cdot L \cdot u_{nw})/K \cdot (\Delta P - t \cdot d\Delta P/dt)^{-1} \quad (6)$$

The position of each saturation at time t is obtained from the Buckley-Leverett equation solved via the method of characteristics:

$$x_f = (qt / A\varphi) \cdot (df_w/ dS_w) \quad (7)$$

where the fractional flow function fw is:

$$f_w = 1 /(1 + (k_{rnw} /\mu_{nw}) \cdot (\mu_w /k_{rw})) \quad (8)$$

The JBN method was originally derived under the assumption of a constant injection rate. When applied to a constant pressure difference experiment, the time-varying total flow rate introduces additional uncertainty into the analytical solution, particularly in the early transient period. The JBN results are therefore used as the initial parameter estimate (base case) as a starting point for the numerical history matching described below and are retained for methodological comparison only.

2.5.2 Numerical approach — Corey model

To address both the compressible gas flow assumption of the JBN method and the variable flow rate arising from the constant pressure difference boundary condition, and additionally to include the effect of capillary forces a numerical history matching interpretation was performed using the 1D numerical core analysis software simulator. The flooding experiment was modelled as a one-dimensional, compressible, immiscible two-phase flow problem. Consistent with the experimental configuration, both the inlet and outlet boundary conditions were specified as Dirichlet pressure conditions, with the inlet pressure set to 7.9 bara and the outlet back-pressure to 3 bara, allowing the total flow rate to vary freely with time as determined by the evolving saturation field and the k_r measurements. The vertical downward flow direction is accounted for by including the gravitational term in the phase velocity expression, with the gravitational component acting in the direction of flow for the denser brine phase and opposing it for hydrogen. Hydrogen density was evaluated using the ideal gas law at the log mean pressure of 5 bar and 20°C. The relative permeability functions were parameterised using the Corey model:

$$k_{rw}(S_w) = k_{rw}^{max} \cdot S_w^{*\,n_w} \quad (9)$$

$$k_{rnw}(S_w) = k_{rnw}^{max} \cdot (1 - S_w^*)^{n_{nw}} \quad (10)$$

where the normalised water saturation S_w^* is defined as:

$$S_w^* = (S_w - S_{wr}) / (1 - S_{nwr} - S_{wr}) \quad (11)$$

and n_w and n_{nw} are the Corey exponents for the water and gas phases respectively, k_{rw}^{max} is the end-point water relative permeability at residual gas saturation, and k_{rnw}^{max} is the end-point gas relative permeability at connate water saturation. The capillary pressure was parameterised using the Brooks-Corey model connected to the k_r estimates with the Burdine tortuosity formulation:

$$P_c(S_w) = P_{cd} \cdot S_w^{*(-1/\lambda)} \quad (12)$$

Where

$$S_w^* = (S_w - S_{wr}) / (1 - S_{wr}) \quad (13)$$

Pcd is the displacement pressure, and λ is the pore size distribution index. All Corey k_r and capillary pressure parameters were adjusted iteratively from the JBN starting point to minimise the sum of squared residuals between the simulated and measured differential pressure and cumulative brine production profiles simultaneously.

3 Results and Discussion

3.1. Petrophysical characterisation

The petrophysical properties of the two core plugs used in this study are summarised in Table 1. For Core 3, the Klinkenberg-corrected gas permeability of 0.460 mD with N2 and 0.522 mD with H_2. For Core 4, the porosity has a 13.31% value, the Klinkenberg-corrected H_2 gas permeability is 0.793 mD and the Klinkenberg-corrected N_2 gas permeability is 0.746 mD. The absolute brine permeabilities are lower than the uncorrected gas permeabilities for both samples. For Core 3, the brine permeability is 0.295 mD 2.3 times relative to Core 4, where the brine permeability was measured to be 0.685 mD. And has a porosity of 13.74%. The uncorrected gas permeability measured with H_2 is lower than the value of N_2 which is physically expected: hydrogen has a smaller molecular diameter and lower viscosity than nitrogen, yielding a higher Klinkenberg slip contribution and therefore a larger apparent permeability before correction. After Klinkenberg correction the two values are expected to converge, and whether any residual difference remains is directly relevant to the proxy gas discussion in Section 3.4.

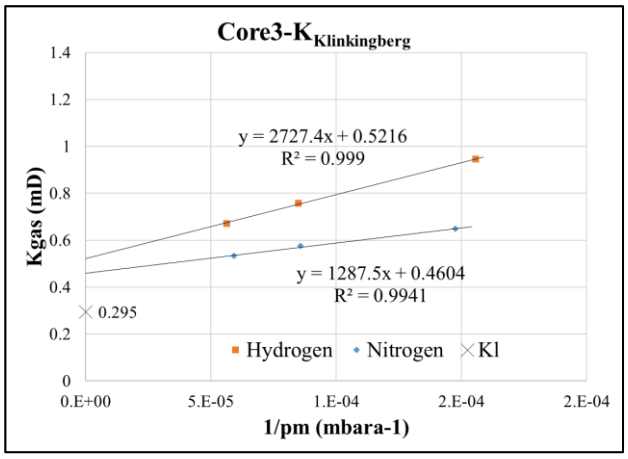

Fig. 2. Klinkenberg-corrected k_g and k_l for Core 3

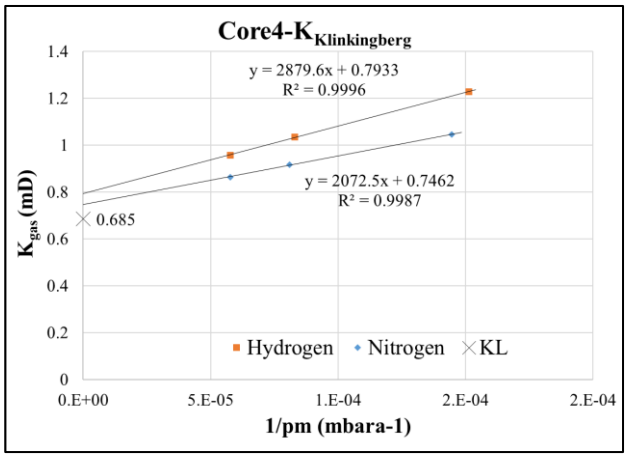

Fig. 3. Klinkenberg-corrected k_g and k_l for Core 4

These reductions for Core 3 are significantly larger and for Core4 somewhat smaller than the approximately 30% suppression of brine permeability relative to gas permeability reported by Maas et al. [17] for clean sandstone, particularly for Core 3 relative to hydrogen permeability, suggesting that fluid-rock interactions in the target formation contribute to the suppression of brine permeability beyond what is expected for a clean system. This has direct consequences for the normalisation of the relative permeability data and for the simulation of hydrogen injectivity, as discussed in Section 3.5. Despite their similar porosities, the two samples show some differences in brine permeabilities, suggesting some differences in pore throat connectivity despite comparable total pore volumes. Both samples fall firmly in the tight range based on their brine permeabilities, directly relevant to their suitability as analogues for aquifers in central Europe, collected from depleted gas reservoir intervals being evaluated as UHS target. Their properties are considerably tighter than Sandstone 2 tested by Rezaei et al. [13], which had a porosity of 10.5% and a liquid permeability of 11.2 mD, reinforcing that the present dataset could provide a piece of the puzzle in trying to fill the gap for a permeability range not previously covered in the published H_2-brine relative permeability literature.

3.2 H_2–brine relative permeability curves

Both measurements were conducted under a constant applied pressure difference of 4.9 bar, with an inlet pressure of 7.9 bara and an outlet back-pressure of 3 bara, giving a log mean pressure of approximately 5 bar at which fluid properties are evaluated. In both cases, hydrogen breakthrough at the outlet was nearly instantaneous, consistent with the highly favourable mobility of hydrogen relative to brine at these conditions. Following breakthrough, the total hydrogen flow rate increased progressively as hydrogen established continuous flow paths through the core, with the increasing hydrogen saturation and its much lower viscosity relative to brine leading to a progressive increase in total system mobility under the constant applied pressure difference. Stable measurement conditions were reached after approximately 320 minutes for Core 3 and 150 minutes for Core 4. The vertical downward flow configuration, with hydrogen injected from the top, was selected to minimise the gravity segregation effects at the inlet reported in horizontal H_2 flooding experiments [12].

3.2.1 JBN analytical results.

The JBN analytical interpretation method was applied as the starting point for the numerical history matching. The end-point gas relative permeability derived from the JBN interpretation is artificially inflated for both samples due to the incompressible flow assumption of the method: hydrogen expands from 7.9 bara to 3 bara across the core with an expansion ratio of approximately 2.6, and the JBN method misinterprets this volumetric acceleration as a high relative permeability rather than correctly attributing it to gas expansion. The JBN results are therefore not reported as standalone parameters but are used solely as the initial estimate for the numerical history matching described below.

Table 3. Corey parameters from the JBN analytical interpretation.

Sample name	Core 3	Core 4
S_{wirr}	0.36	0.51
$S_w(S_{gi}=0)$	1	1
$k_{rg}(S_{wirr})$	0.088	0.130
$k_{rw}(S_w=1)$	1	1
n_w	3	4
n_g	2.5	1

3.2.2 Corey numerical history matching results

The Corey relative permeability and Brooks-Corey capillary pressure parameters are interpreted from numerical history matching.
The history match for Core 3 and Core 4 yields the parameters given and are summarised in Tables 4 and 5. These results have not been calibrated to the Corey values estimated by the JBN analytical interpretation method, since JBN neglects the capillary forces. The JBN k_r estimates were used and plotted as an initial guess (base case) for the starting point of the numerical history match.

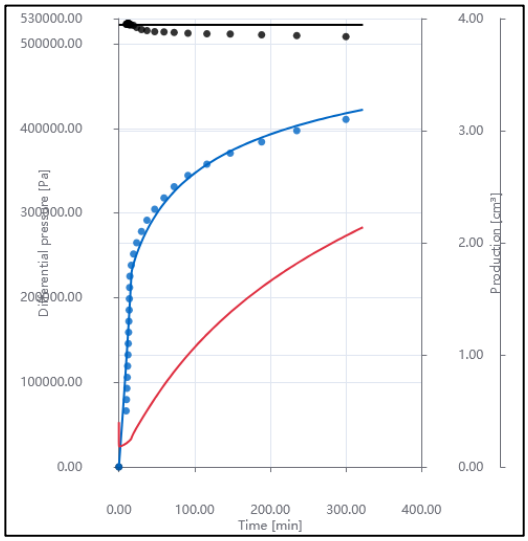

Fig. 4. Simulated (solid line) and measured (dotted line) cumulative brine production(blue) and differential pressure(black) for Core 3.

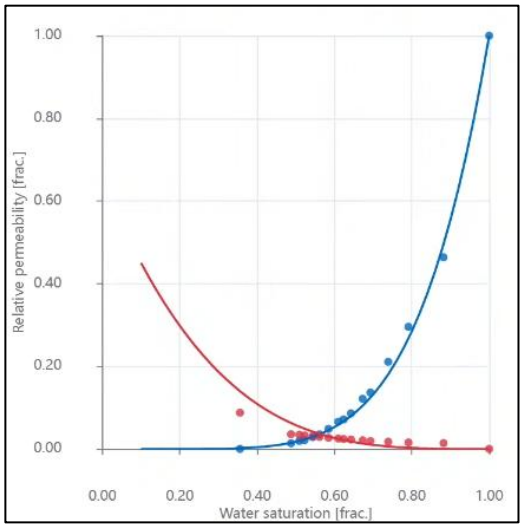

Fig. 5. Corey-estimated k_{rg}(red solid line) k_{rw}(blue solid line) and the numerical history matching interpretation and JBN represent as points for Core 3

The history match for Core 3 is shown in Fig.4., Fig.5. and for Core 4 is shown in Fig.6., Fig.7. the comparison of relative permeability estimates in Fig.9. and as well as the synthetic capillary pressure for both in Fig.8. The simulated differential pressure, cumulative brine production, and time-varying gas injection rate all match the experimental data closely throughout the entire flooding period, confirming that the compressible flow formulation and fluid properties evaluated at the log mean pressure of 5 bar and 20°C are consistent with the experimental observations. Both experiments were conducted as primary drainage from full brine saturation, with S_w=1.000 and S_{gi}=0 for both samples.

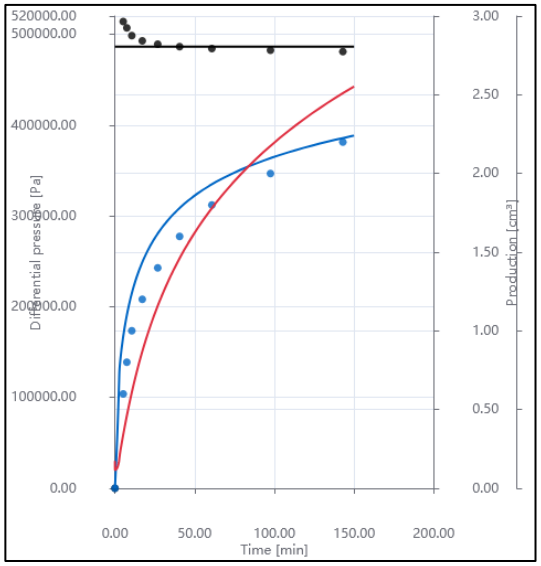

Fig. 6. Simulated (solid line) and measured (dotted line) cumulative brine production(blue) and differential pressure(black) for Core 4.

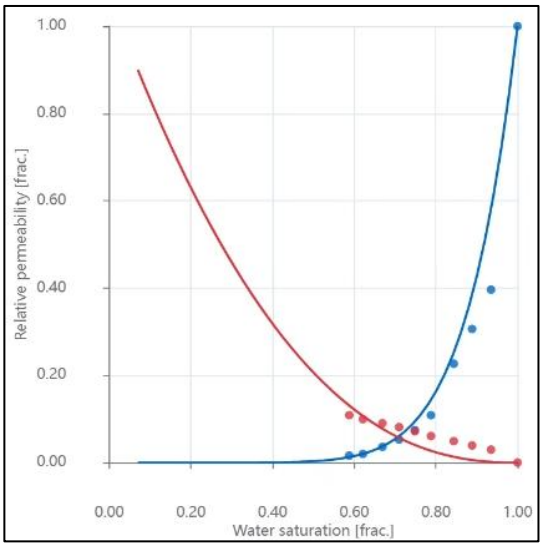

Fig. 7. Corey-estimated k_{rg}(red solid line) k_{rw}(blue solid line) and the numerical history matching interpretation and JBN represent as points for Core 4

For Core 3, S_{wirr}=0.100 and $k_{rg}(S_{wirr})$=0.450, indicating a substantially lower gas end-point and higher extrapolated irreducible water saturation in the tighter sample with the measured value of 36% remaining brine indicated by the last JBN value. The Corey model for Core 4 yields to an

extrapolated value of irreducible water saturation of S_{wirr}=0.070, where the last JBN value indicating that approximately 58% of the pore volume remains brine-occupied at the end of a primary drainage injection cycle. This could be explained by the nature of the dynamic flooding experiment and the significant viscosity difference between the displacing and the displaced fluid. The fractional flow of water is shown for both cores in Fig. 10.

Table 4. Corey k_r parameters from the numerical history matching interpretation.

Sample name	C3B2_05_RP	C4B6_03_RP
S_{wirr}	0.10	0.07
S_{w1}	1.00	1.00
$k_{rg}(S_{wirr})$	0.45	0.90
$k_{rw}(S_{gi})$	1.00	1.00
n_w	5.00	7.50
n_g	3.50	2.37

Table 5. Brooks-Corey (with Burdine k_r correlation) capillary pressure parameters from the numerical history matching interpretation.

Sample name	Core 3	Core 4
P_{cd} [Pa]	100,000	110,000
λ	3.00	4.00
S_{wirr}	0.10	0.07

The end-point gas relative permeability $k_{rg}(S_{wirr})$=0.900 indicates that at irreducible water saturation, the effective hydrogen permeability reaches 90% of the absolute gas permeability reference. The end-point water relative permeability $k_{rw}(S_{gi})$ =1.000 is equal to unity by definition, as it represents the water permeability at the initial condition of zero gas saturation. The high n_w value of 7.50 describes a strongly concave brine k_r curve, with brine mobility remaining very low across most of the saturation range and rising steeply only as S_w approaches unity. The n_g value of 2.37 describes a moderately convex hydrogen k_r curve, with hydrogen mobility building progressively from breakthrough onward. This combination is characteristic of a strongly water-wet system with a high mobility contrast between the two phases, consistent with the physical properties of the H_2-brine system at the experimental conditions.

The Corey shape parameters reveal a strongly asymmetric k_r behaviour between the two phases for Core 4.

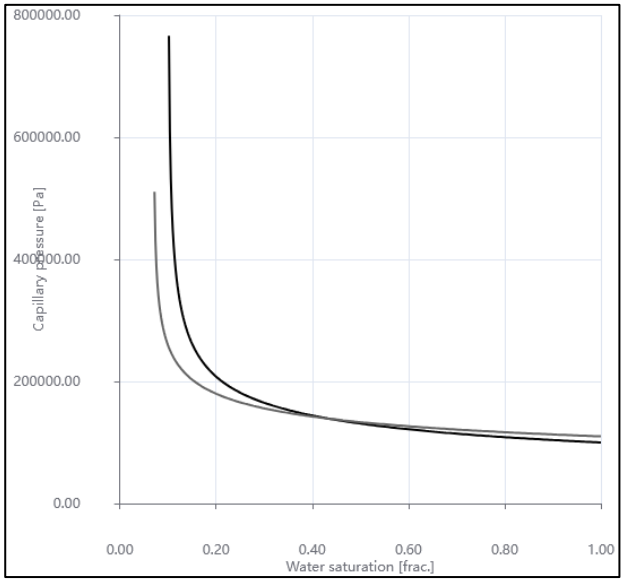

Fig. 8. Brooks-Corey synthetic capillary pressure curves applied in the numerical history matching interpretation for Core 3(black solid line) and 4(grey solid line)

The Brooks-Corey capillary pressure parameterisation obtained from numerical simulation for Core 3 and Core 4 yields a displacement pressure of Pcd=0.10MPa and 0.11MPa and a pore size distribution index of λ=3.00 and 4.00 respectively.

The large displacement pressure reflects the tight pore throat size of this sample, consistent with its low brine permeability of 0.685 mD. The inclusion of an accurate capillary pressure description in the history matching workflow is critical for these tight samples. The strong capillary pressure gradient near the outlet of the core creates a significant capillary end effect, where the wetting phase is retained at the outlet face at a higher saturation than in the remainder of the core. Failure to account for this end effect leads to an overestimation of S_{wirr} and an underestimation of $k_{rg}(S_{wirr})$ [17]. The extrapolated irreducible brine saturations and therefore the extrapolated endpoint carry high uncertainty without true measured capillary pressure. This additional data would provide and improvement of the simulation results in the numerical history matching workflow.

3.3 Effect of permeability on k_r estimates

A comparison of the Corey parameters between Core 3 and Core 4 reveals a systematic dependence of the k_r endpoints and curve shape on sample permeability, despite their similar porosities. Core 4, with the higher brine permeability of 0.685 mD, yields S_{wirr}=0.070 and $k_{rg}(S_{wirr})$=0.900, while the tighter Core 3, with a brine permeability of 0.295 mD, yields S_{wirr}=0.100 and $k_{rg}(S_{wirr})$=0.450. The higher irreducible water saturation in the tighter Core 3 is consistent with the expectation that tighter pore systems retain a larger fraction of brine within smaller pore throats due to stronger capillary forces. The

corresponding reduction in end-point gas relative permeability reflects the more restricted and tortuous hydrogen flow pathways available at irreducible water saturation in the tighter sample.

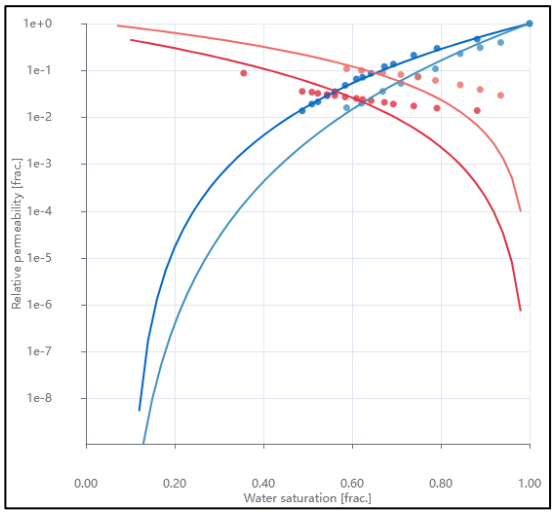

Fig. 9. Comparison of relative permeability estimates from the in the numerical history matching interpretation (solid lines) and from JBN (points) for Core 3(bright shade) and 4(dark shade)

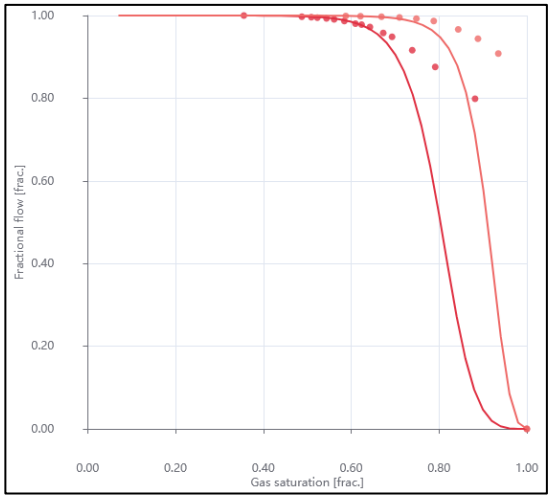

Fig. 20. Fractional flow curves applied in the numerical history matching interpretation for Core 3(bright red solid line) and 4(dark red solid line)

The Corey shape parameters also differ between the two samples. The n_w value of 5.00 for Core 3 compared to 7.50 for Core 4 indicates a less strongly concave brine relative permeability curve in the tighter sample, while the ng value of 3.50 for Core 3 compared to 2.37 for Core 4 reflects a more gradual development of hydrogen mobility from breakthrough onward. In both samples, the relative permeability behaviour remains strongly asymmetric between the wetting and non-wetting phases, characteristic of a strongly water-wet hydrogen–brine system with a substantial mobility contrast between the two fluids.

These differences in relative permeability behaviour are expected to influence predicted injectivity profiles, pressure response, and hydrogen sweep behaviour during underground hydrogen storage operations in aquifers or in a depleted hydrocarbon reservoir with high water saturation. The observed variability between the two samples indicates that a single representative saturation dependent relative permeability may not adequately capture the flow behaviour of heterogeneous tight sandstone storage formations and that permeability-dependent parameterisation should be considered in field-scale simulation workflows.

The reduction factor between corrected k_{gas} and k_{brine} also differs between the samples, suggesting that the mechanisms responsible for brine permeability suppression are not uniform across the formation. This heterogeneity in the relationship between gas and brine permeability has direct implications for the permeability normalisation correction discussed in Section 3.5 and suggests that renormalisation may need to be applied on a sample-specific or flow-unit basis rather than through a single formation-wide correction factor.

3.4 Comparison with literature — CO_2–brine and N_2–brine analogues

The H_2–brine relative permeability results derived in this study are placed in the context of published H_2–brine, N_2–brine, and CO_2–brine datasets to assess the extent to which analogue gas systems can substitute for H_2–brine measurements in underground hydrogen storage simulation workflows. The irreducible water saturation obtained for Core 4, the extrapolated S_{wirr}=0.070, is substantially lower than the approximately 40% reported by Yekta et al. [10] under steady-state conditions and lower than the values approaching 60% reported by Lysyy et al. [11] and Boon and Hajibeygi [12] for higher-permeability Berea sandstone samples. Several factors specific to the present study may contribute to this difference. The results of all listed papers are coming from dynamic experiments and such low irreducible saturations are not achievable because of the limited pressure difference generated during the flooding. In order to achieve the “true” S_{wirr} static experiments are needed, such as porous plate or centrifuge. In the presented case, the S_{wirr} was anchored to the provided value. The values in this study reported for the remaining brine saturations, 36% and 58% are somewhat in agreement with the ones reported in the available literature. The constant pressure difference protocol continuously drives the primary drainage process and promotes further brine displacement compared to steady-state methods, where capillary equilibrium is established at each injection step. In addition, the numerical history matching workflow explicitly accounts for capillary end effects through the coupled Corey relative permeability and Burdine correlated Brooks-Corey capillary pressure parameterisation. Failure to account for these end effects in tight rocks may lead to overestimation of irreducible water saturation and underestimation of gas relative permeability endpoints. The experiments of Rezaei et al.

[13] were conducted at elevated pressure and temperature conditions (20.68 MPa and 353 K), whereas the present measurements were performed at a log mean pressure of approximately 5 bar and 20°C. Rezaei et al. [13] reported that hydrogen relative permeability behaviour varies with pressure due to changes in hydrogen viscosity and interfacial properties with brine, and direct quantitative comparison between datasets obtained under substantially different thermodynamic conditions should therefore be approached with caution. Measurements at representative reservoir pressure and temperature conditions are recommended before the relative permeability functions derived here are applied directly to deeper underground hydrogen storage scenarios. Rezaei et al. [13] also investigated whether N_2 can serve as a practical proxy for H_2 in primary drainage relative permeability experiments. Their results showed that H_2 and N_2 produced broadly similar gas relative permeability behaviour during primary drainage, while CH_4 exhibited higher relative permeability at intermediate saturations but lower end-point mobility. However, Thaysen et al. [14] demonstrated through pore-scale imaging that H_2 recovery behaviour during imbibition differs significantly from N_2, suggesting that N_2 may not be an appropriate proxy when residual trapping and hysteresis effects are of interest. The Klinkenberg-corrected permeability comparison between H_2 and N_2 presented in Table 1 provides evidence about the questioned suitability of N_2 as a proxy gas at the single-phase permeability level for this specific rock type. Boon et al. [15] showed that during storage periods hydrogen ganglion sizes may increase due to Ostwald ripening, reducing residual saturation and relative permeability hysteresis, which could improve working gas recovery during cyclic operations. Similar observations were reported by Goodarzi et al. [16]. These processes affect imbibition relative permeability and capillary pressure behaviour, which were not investigated in the present study but should be incorporated into future cyclic underground hydrogen storage simulation workflows to evaluate trapping losses over repeated injection–withdrawal cycles. Across the available literature, most published H_2–brine relative permeability datasets have been obtained on comparatively high-permeability rocks under conditions representative of saline aquifer storage. In contrast, the present study focuses on tight sandstone samples representative of possible aquifers collected from depleted gas reservoir intervals examined for underground hydrogen storage in central Europe. The comparison across available datasets therefore reinforces the conclusion that rock type, pore structure, and thermodynamic conditions exert a dominant control on H_2–brine relative permeability behaviour and highlights the importance of formation-specific experimental measurements for reliable underground hydrogen storage simulation.

3.5 Implications for UHS simulation

The H_2–brine relative permeability functions derived in this study have direct and practical implications for the numerical simulation of underground hydrogen storage operations in the target formation. Three engineering aspects are considered: injectivity and pressure management, the implications of gas type and proxy gas selection, and the choice of reference permeability for simulation input.

3.5.1 Injectivity, pressure management, and displacement behaviour.

The end-point hydrogen relative permeability of $k_{rg}(S_{wirr})=0.900$ for Core 4 and $k_{rg}(S_{wirr})=0.450$ for Core 3 indicates that once the formation is drained to irreducible water saturation, hydrogen mobility becomes strongly dependent on the permeability structure of the rock. The high gas end-point relative permeability observed in Core 4 suggests relatively high hydrogen mobility once continuous gas pathways are established, whereas the lower gas endpoint in Core 3 reflects the stronger capillary restriction associated with the tighter pore system. The strong characteristics of brine relative permeability curves observed in both samples indicate that brine mobility decreases rapidly as hydrogen saturation increases. This behaviour is expected to restrict brine counterflow during cyclic injection and withdrawal operations and should therefore be considered during pressure management analysis in underground hydrogen storage simulation workflows. The lower n_g value observed for Core 4 additionally indicates a more rapid development of hydrogen mobility following breakthrough compared to Core 3, which may favour injectivity but could also promote earlier transition to hydrogen-dominated flow behaviour. The mobility ratio between hydrogen and brine is a critical parameter governing displacement stability during hydrogen injection. Hagemann [18] estimated H_2–water mobility ratios between 2 and 5 for porous reservoir systems and identified viscous fingering and gravity override as important instability mechanisms during hydrogen injection. Although the present experiments were conducted at the core scale and do not directly reproduce field-scale displacement processes, the rapid development of hydrogen mobility observed during primary drainage is consistent with the possibility that similar instability mechanisms may become relevant during field-scale underground hydrogen storage operations. The primary drainage experiments were initiated from fully brine-saturated conditions, with no initial hydrogen saturation present in the pore space. The resulting irreducible water saturations indicate that a fraction of the pore volume remains inaccessible to hydrogen following primary drainage, thereby reducing the effective working gas storage volume available during injection cycles. Residual hydrogen trapping during re-imbibition is governed by imbibition relative permeability and capillary pressure behaviour, which were not measured in the present study. Previous pore-scale studies have shown that hydrogen recovery during imbibition decreases with increasing pressure and that Ostwald ripening during storage periods may reduce residual saturation and relative permeability hysteresis, potentially improving hydrogen recovery efficiency during cyclic operation [15,16]. Hagemann [18] additionally

demonstrated that microbial energy losses during cyclic underground hydrogen storage operation may become significant due to microbial hydrogen consumption at the hydrogen concentration front within the reservoir. The sweep efficiency of hydrogen through the formation, and therefore the contact time between injected hydrogen and hydrogenotrophic microorganisms, is strongly influenced by the relative permeability behaviour of the system.
Accurate experimental relative permeability data are therefore important not only for hydrodynamic simulation of underground hydrogen storage operations but also for coupled bio-reactive simulation workflows addressing microbial hydrogen losses.

3.5.2 Implications of gas type on kr and the use of proxy gases

Rezaei et al. [13] reported that H_2 and N_2 produced broadly similar gas relative permeability behaviour during primary drainage experiments conducted at reservoir conditions, leading those authors to suggest N_2 as a practical proxy gas for primary drainage flow experiments. However, CH_4 exhibited systematically different behaviour at intermediate saturations and lower end-point mobility. Furthermore, Thaysen et al. [14] demonstrated that H_2 recovery during imbibition differs significantly from N_2, suggesting that N_2 may not be an appropriate analogue when residual trapping and hysteresis behaviour are important. In the context of underground hydrogen storage simulation, the choice of proxy gas also affects predictions of gas mixing behaviour between injected hydrogen and the resident cushion gas phase, which may consist of natural gas, methane-rich gas, or residual hydrogen. These mixing processes are sensitive to the relative mobility of the gas phases and to the underlying two-phase flow behaviour of the system. Proxy gas experiments alone may therefore not fully capture the flow behaviour relevant to underground hydrogen storage operations and should ultimately be validated against formation-specific H_2–brine measurements such as those presented in this study. The comparison between Klinkenberg-corrected H_2 and N_2 permeabilities presented in Table 1 provides additional supporting information regarding questioning the suitability of N_2 as a proxy gas already at the single-phase permeability level for this specific formation.
Considering the complexity of multiphase fluid flow and the amount of available datapoints suggests that additional experiments are of necessity to draw a conclusion whether application of proxy gas data is a suitable option when it comes to H_2-brine relative permeability values.

3.5.3 Implications for permeability normalisation and simulator implementation

The substantial discrepancy between gas permeability and brine permeability observed in both samples has direct implications for relative permeability normalisation and simulator implementation. In the present study, Klinkenberg-corrected gas permeabilities exceed the corresponding brine permeabilities, the values deviate form the approximately 30% reduction reported by Maas et al. [17] for cleaner sandstone systems. This behaviour suggests that fluid–rock interactions and pore-scale effects specific to the investigated formation significantly suppress brine permeability relative to gas flow. When normalised to brine permeability, systems with substantially higher gas permeability may yield gas relative permeability values approaching or exceeding unity. Such behaviour creates practical complications in commercial reservoir simulators, some of which assume that relative permeability values remain below one. Maas et al. [17] demonstrated that this issue can be resolved by renormalising the relative permeability curves to the Klinkenberg-corrected gas permeability rather than to the brine permeability. This approach preserves the underlying flow behaviour while maintaining physically consistent scaling for simulator implementation. The results of the present study also raise attention to this recommendation for tight hydrogen storage formations where the discrepancy between gas and brine permeability is large. The variability observed between Core 3 and Core 4 further indicates that the relationship between gas permeability and brine permeability is not uniform across the formation. Permeability renormalisation corrections should therefore be applied on a sample-specific or flow-unit basis rather than through a single formation-wide correction factor. Failure to account for this heterogeneity may introduce uncertainty into predicted injectivity and pressure response during underground hydrogen storage simulation.

4 Conclusions & Future Work

This study presents experimental H_2-brine primary drainage relative permeability measurements on two tight sandstone core plugs from the North German Basin, with brine absolute permeabilities of 0.295 mD and 0.685 mD, representative of depleted gas reservoir intervals considered for underground hydrogen storage. Unsteady-state core flooding experiments were conducted under constant pressure difference conditions in a laboratory approved for hydrogen use at 20°C, and relative permeability functions were derived using numerical history matching with a Corey relative permeability and Brooks-Corey capillary pressure formulation (with Burdine k_r correlation) accounting for hydrogen compressibility and capillary end effects. The following conclusions are drawn. The numerical history matching results indicate a pronounced dependence of hydrogen–brine relative permeability behaviour on sample permeability, despite the similar porosities of the investigated core plugs. Core 4 yields S_{wirr}=0.070, $k_{rg}(S_{wirr})$=0.900, n_w=7.50, and n_g=2.37, while the tighter Core 3 yields S_{wirr}=0.100, $k_{rg}(S_{wirr})$=0.450, n_w=5.00, and n_g=3.50. The relative permeability behaviour observed in both samples is strongly asymmetric between the wetting and non-wetting phases, with strongly decreasing brine relative permeability and progressively increasing hydrogen mobility during primary drainage, consistent with a strongly water-wet hydrogen–brine system

characterised by a substantial mobility contrast between the phases. The absolute brine permeabilities of both samples are substantially lower than the corresponding gas permeabilities, with reduction factors for Core 4 considerably exceeding the approximately 30% suppression reported for cleaner sandstone systems. This behaviour suggests significant fluid–rock interactions specific to the target formation. The discrepancy between gas and brine permeability has direct implications for relative permeability normalisation and simulator implementation, therefore this is recommended to pay attention to before the data are applied in field-scale underground hydrogen storage simulation workflows. The results in comparison to other studies additionally demonstrate pronounced permeability dependence of the relative permeability and capillary pressure behaviour, indicating that directly transferring relative permeability functions between samples or from analogue gas systems without permeability-specific correction may introduce uncertainty into predicted injectivity, pressure evolution, and working gas capacity. The measured and estimated results of this study serve as a piece of the puzzle. The formation-specific hydrogen–brine relative permeability and capillary pressure functions reported here provide quantitative two-phase flow input for hydrodynamic and coupled bio-reactive underground hydrogen storage simulation workflows, addressing a limitation previously identified in field-scale predictive modelling of underground hydrogen storage systems. Future work should extend these measurements to imbibition conditions and to representative reservoir pressure and temperature conditions in order to quantify residual hydrogen trapping, relative permeability hysteresis during cyclic primary drainage–imbibition operation, and the pressure dependence of hydrogen–brine flow behaviour. A wider selection of core samples varying the petrophysical properties is necessary to complete the dataset to draw ultimate conclusions for the questioned raised through this study. As well as comparison against pore-scale modelling outcomes, which consider the pore structure and interfacial interactions could help. A systematic comparison between saline aquifer and depleted gas reservoir storage scenarios, including the role of mixing zones between injected hydrogen and residual cushion gas, would further improve the applicability of these data to field-scale underground hydrogen storage design.

Acknowledgments

The authors thank Prof. Andreas Henk, Sonu Roy and the Institute of Applied Geosciences at Technische Universität Darmstadt for providing the core plug samples through Eberhard Jahns from Gesteinslabor Jahns Gmbh.

References

1. N. Johnson et al., Nat. Rev. Clean Technol., 1, 351–371 (2025).
2. Y. Mathur et al., International Journal of Hydrogen Energy, 165 (2025).
3. B. Parkinson et al., Energy Environ. Sci., 12 (2019).
4. M. Lardhi et al., International Journal of Hydrogen Energy, 101 (2025).
5. K. Opoku Duartey et al., Energies, 18, 748 (2025).
6. J.M. Miocic et al., Geological Society, London (2023).
7. S. Youssef, Unlocking the Subsurface H_2 Production and Storage Potential: R&D Challenges and Technological Pathways from RCA and SCAL Perspectives, 38th International Symposium of the Society of Core Analysts, Hannover, Germany, August 25–28, 2025. (IFPEN)
8. I. Gomez Mendez et al., Energy and Fuels, 21 (2024).
9. J. Michelsen et al., H2020 HyUSPRe Project Report, 67 pp (2023).
10. A.E. Yekta et al., Transport in Porous Media, 122, 333–356 (2018).
11. M. Lysyy et al., Geophysical Research Letters, 49 (2022).
12. M. Boon and H. Hajibeygi, Scientific Reports, 12 (2022).
13. A. Rezaei et al., Geophysical Research Letters, 49, e2022GL099433 (2022). https://doi.org/10.1029/2022GL099433
14. M. Thaysen et al., International Journal of Hydrogen Energy, 48 (2023).
15. M. Boon et al., Scientific Reports, 14 (2024).
16. S. Goodarzi et al., International Journal of Hydrogen Energy, 56 (2024).
17. J.G. Maas, D. Santonico, A. Hebing, N. Springer, Defining absolute permeability for CO_2 injection projects: scope for increased economic storage capacity, SCA2025-1037, 36th International Symposium of the Society of Core Analysts (2025).
18. B. Hagemann, Numerical and Analytical Modeling of Gas Mixing and Bio-Reactive Transport during Underground Hydrogen Storage, Schriftenreihe des Energie-Forschungszentrums Niedersachsen (EFZN), Cuvillier Verlag, ISBN 9783736997141 (2018).
19. E.F. Johnson, D.P. Bossler, V.O.N. Bossler, Calculation of relative permeability from displacement experiments, Transactions of the AIME, 216, 370–372 (1959). https://doi.org/10.2118/1023-G
20. S.C. Jones and W.O. Roszelle, Graphical techniques for determining relative permeability from displacement experiments, Journal of Petroleum Technology, 30, 807–817 (1978). https://doi.org/10.2118/6045-PA
21. C. McPhee, J. Reed, I. Zubizarreta, Best Practice in Coring and Core Analysis, Developments in Petroleum Science, 64, 1–15 (2015). https://doi.org/10.1016/B978-0-444-63533-4.00001-9